
ACCELERATING NEURAL ODE BASED CNN MODELS ON LOW-COST FPGAs

A PREPRINT

Hirohisa Watanabe

Keio University
3-14-1 Hiyoshi, Kohoku-ku, Yokohama, Japan
watanabe@arc.ics.keio.ac.jp

Hiroki Matsutani

Keio University
3-14-1 Hiyoshi, Kohoku-ku, Yokohama, Japan
matutani@arc.ics.keio.ac.jp

December 22, 2024

ABSTRACT

ODENet is a deep neural network architecture in which a stacking structure of ResNet is implemented with an ordinary differential equation (ODE) solver. ANODE is an extended approach of ODENet for stably high accuracy by introducing more precise training algorithm using more memory in training phase. It is also possible to improve the accuracy while keeping the same number of parameters on resource-limited edge devices. In this paper, using Euler method as an ODE solver, a part of ODENet and ANODE are implemented as a dedicated logic on a low-cost FPGA (Field-Programmable Gate Array) board, such as PYNQ-Z2 board. As ODENet variants, reduced ODENets (rODENets) each of which heavily uses a part of ODENet layers and reduces/eliminates some layers differently are proposed and analyzed for low-cost FPGA implementation. In addition, rANODE is proposed as an ANODE variant in a way similar to the rODENet. They are evaluated in terms of parameter size, accuracy, execution time, and resource utilization on the FPGA. The results show that an overall execution time of rODENet and rANODE variants is improved by up to 2.66 times compared to a pure software execution while keeping a comparable accuracy to the original ODENet and ANODE.

Keywords CNN · DNN · ResNet · Neural ODE · FPGA

1 Introduction

ResNet [1] is a well-known deep neural network (DNN) architecture with high accuracy. In addition to conventional forward propagation of DNNs, it has shortcut or skip connections that directly add the input of a layer to the output of the layer. Since it can mitigate vanishing and exploding gradient problems, we can stack more layers to improve prediction accuracy. However, stacking many layers increases the number of parameters of DNNs; in this case, memory requirement becomes severe in resource-limited edge devices.

ODENet [2] that employs an ordinary differential equation (ODE) solver in DNNs was proposed to reduce weight parameters of the network. Stacking structure of layers in ResNet can be represented with an ODE solver, such as Euler method. ODENet thus uses an ODE solver in prediction and training processes so that M layers in ResNet are replaced with M repeated executions of a single layer, as shown in Figures 1 and 2. In this case, ODENet can significantly reduce the number of parameters compared to the original ResNet while keeping the equivalent prediction and training processes. However, there is still an issue on stability of the training process of ODENet. ANODE [3] is an extended approach of ODENet to address this issue by introducing a checkpointing technique that can compute more precise gradients but using more memory in the training phase.

Field-Programmable Gate Array (FPGA) is an energy-efficient solution, and it has been widely used in edge devices for machine learning applications. In this paper, we thus propose an FPGA-based acceleration of ODENet. A core component of ODENet, called ODEBlock, that consists of convolution layers, batch normalization [4], and activation function is implemented on a programmable logic of low-cost FPGA board, such as PYNQ-Z2 board. Our contribution

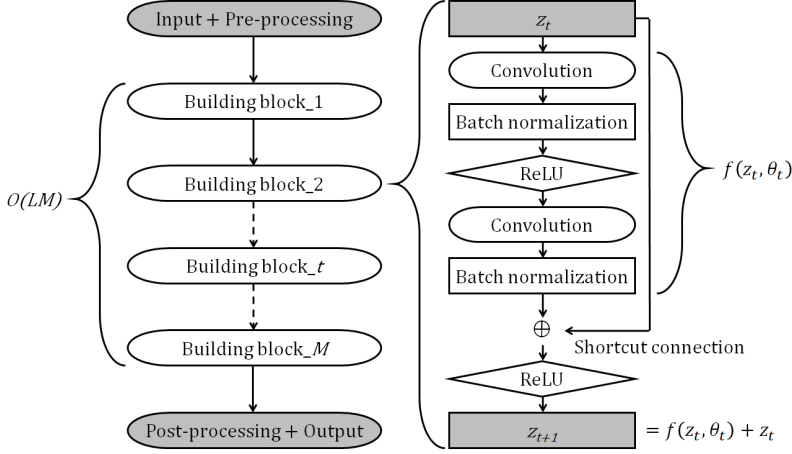


Figure 1: ResNet architecture

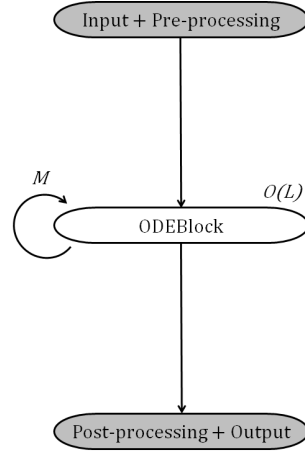


Figure 2: ODENet architecture

is that, as ODENet variants, reduced ODENets (rODENets) each of which heavily uses a part of ODEBlocks and reduces/eliminates some layers differently are proposed and analyzed for low-cost FPGA implementation. Reduced ANODEs (rANODEs) are also proposed as well. They are evaluated in terms of parameter size, accuracy, execution time, and resource utilization on the FPGA ¹.

Many studies on FPGA-based DNN accelerators have been reported. In [6], such accelerators and their techniques, such as binarization and quantization, are surveyed. When a quantization using 2-bit weight parameters is applied to ResNet-18, 10.3% accuracy loss is reported. In [7], circuit techniques that minimize information loss from quantization are proposed and applied to ResNet-18 and 50. In [8], ResNet-50 and 152 are implemented on Intel Arria-10 FPGA using a 16-bit format and external memories. Microsoft Brainwave platform supports ResNet-50 [9]. Please note that this work focuses on low-cost FPGA platforms, such as PYNQ-Z2. Also our approach is orthogonal to quantization techniques and can be combined with for further reducing the parameter sizes.

The rest of this paper is organized as follows. Section 2 provides a brief review of basic technologies about ODENet and ANODE. Section 3 implements a building block of ODENet and ANODE on the FPGA, and Section 4 shows the evaluation results. Section 5 concludes this paper.

2 Preliminaries

2.1 ResNet

In neural networks that serially stack many layers, training process may be prevented when gradients become vanishingly small in one of the layers (i.e., vanishing gradient problem). Also, there may be a possibility that the training becomes unstable when gradient descent is diverging (i.e., exploding gradient problem). ResNet [1] was proposed to address these issues and improve the prediction accuracy by introducing shortcut connections that enable to stack many layers. Figure 1 illustrates ResNet architecture. As shown in the figure, ResNet consists of a lot of building blocks. Each building block receives input data z_t and executes 3×3 convolution, batch normalization [4], ReLU [10] as an activation function, 3×3 convolution, and batch normalization. For example, ResNet architecture, which will be shown in Table 4, can be used in image classification tasks, such as CIFAR-10 and CIFAR-100 datasets. In this paper, building blocks executing the same computations are grouped as layer x , where $x = 1, 2, 3$. ResNet size is denoted as ResNet- N , where N is the total number of convolution and fully-connected steps in the building blocks including the pre- and post-processing layers.

Let $z \in \mathbb{R}^Z$ and $y \in \mathbb{R}^Z$ be an input and an output of ResNet, respectively. A network parameter θ is interpreted as a mapping function $\mathcal{H} : z \rightarrow y$. Assuming a normal forward propagation, an output of a building block is represented as a function $f(z, \theta)$. When an input of a building block is additionally added to an output of the building block with a shortcut connection, the function is changed to $f(z, \theta) + z$. Even with a shortcut connection, an output of the building block itself is still $\mathcal{H}(z)$. Thus, its residual should be trained in the training process so that $f(z, \theta) = \mathcal{H}(z) - z$. In this case, a gradient at least contains 1; thus, vanishing gradient problem can be mitigated.

¹This paper is an extended version of our international workshop paper [5] by newly proposing rANODE variants.

Assuming ResNet consists of multiple building blocks, an input to the $(t + 1)$ -th building block is represented as follows.

$$\mathbf{z}_{t+1} = \mathbf{z}_t + f(\mathbf{z}_t, \theta_t), \quad (1)$$

where \mathbf{z}_t and θ_t denote the input and parameter of the t -th building block, respectively.

2.2 Ordinary Differential Equation

ODE is an equation containing functions of one variable and their derivatives. For example, a first-order differential equation is represented as follows.

$$\frac{dz}{dt} = f(z(t), t, \theta), \quad (2)$$

where f and θ represent dynamics and the other parameters, respectively. Assuming f is known and $z(t_0)$ is given, a problem to find $z(t_1)$ that satisfies the above equation is known as an initial value problem. It is formulated as follows.

$$z(t_1) = z(t_0) + \int_{t_0}^{t_1} f(z(t), t, \theta) dt \quad (3)$$

$$= \text{ODESolve}(z(t_0), t_0, t_1, f) \quad (4)$$

In the right side of Equation 3, the second term contains an integral of a given function. It cannot be solved analytically for arbitrary functions, so a numerical approximation is typically employed to solve Equation 3. To solve the equation, ODESolve function is defined as shown in Equation 4. In ODESolve function, integration range $[t_0, t_1]$ is divided into partitions with step size h . For $t_0 < \dots < t_i < \dots < t_1$, it computes corresponding z_i using a recurrence formula. As a method to compute $z(t_1)$ in Equation 4, well-known ODE solvers, such as Euler method, second-order Runge-Kutta method, and fourth-order Runge-Kutta method, can be used [11]. They can approximately solve Equation 3 in the first-order, second-order, and fourth-order accuracy, respectively. Below is Euler method.

$$z(t_{i+1}) = z(t_i) + hf(z(t_i), t_i, \theta) \quad (5)$$

2.3 ODENet

An output of building blocks in ResNet can be computed with a recurrence formula, as shown in Equation 1. Please note that Equation 1 is similar to Equation 5 except that the former basically assumes vector values while the latter assumes scalar values. Thus, one building block is interpreted as one step in Euler method. As mentioned in Section 2.2, since Euler method is a first-order approximation of Equation 3, an output of ResNet building block can be interpreted as well. Since Equation 3 can be solved by Equation 4, the output of ResNet can be solved by the same equation. Here, a building block of ResNet is replaced with an ODEBlock using ODESolve function. Neural network architecture consisting of such ODEBlocks is called ODENet. Figure 2 shows an ODENet architecture. ODENet that repeats the same ODEBlock M times is interpreted as ResNet that implements M building blocks.

Prediction tasks of ODENet are executed based on Equation 4. In training process, it is required that gradients are back-propagated along neural network layers via ODESolve function. To compute the gradients, ODENet uses an adjoint method [12] in the training process. Here, loss function J of ODENet is represented as follows.

$$J(\mathbf{z}(t_1)) = J(\text{ODESolve}(\mathbf{z}(t_0), t_0, t_1, f)) \quad (6)$$

Let an adjoint vector \mathbf{a} be $\mathbf{a} = \frac{\partial J}{\partial \mathbf{z}(t)}$. The following equation is satisfied with respect to \mathbf{a} .

$$\frac{d\mathbf{a}(t)}{dt} = -\mathbf{a}^\top \frac{\partial f(\mathbf{z}(t), t, \theta)}{\partial \mathbf{z}(t)} \quad (7)$$

Based on Equations 7 and 4, a gradient of parameter θ derived by a loss function is computed as follows.

$$\begin{aligned} \frac{dJ}{d\theta} &= - \int_{t_1}^{t_0} \mathbf{a}(t)^\top \frac{\partial f(\mathbf{z}(t), t, \theta)}{\partial \theta} dt \\ &= \text{ODESolve} \left(\mathbf{0}, t_1, t_0, -\mathbf{a}(t)^\top \frac{\partial f(\mathbf{z}(t), t, \theta)}{\partial \theta} \right) \end{aligned} \quad (8)$$

$\mathbf{z}(t)$ and $\mathbf{a}(t)$ can be computed with ODESolve function. A training function can be summarized as follows by using Equation 8 and these values [2].

$$\begin{aligned} \mathbf{z}(t_0) &= \text{ODESolve}(\mathbf{z}(t_1), t_1, t_0, f(\mathbf{z}(t), t, \theta)) \\ \mathbf{a}(t_0) &= \text{ODESolve}\left(\mathbf{a}(t_1), t_1, t_0, -\mathbf{a}(t)^\top \frac{\partial f(\mathbf{z}(t), t, \theta)}{\partial \mathbf{z}(t)}\right) \\ \frac{dJ}{d\theta} &= \text{ODESolve}\left(\mathbf{0}, t_1, t_0, -\mathbf{a}(t)^\top \frac{\partial f(\mathbf{z}(t), t, \theta)}{\partial \theta}\right) \end{aligned} \quad (9)$$

Please note that vector size of $\mathbf{0}$ in Equation 9 is same as that of θ . In the original Equation 8, it is necessary to compute $\mathbf{a}(t)$ and $\mathbf{z}(t)$ for each t . On the other hand, in the case of Equation 9, $\mathbf{z}(t)$ is computed first using ODESolve function; then $\mathbf{a}(t)$ is computed based on $\mathbf{z}(t)$, and the gradient is computed based on $\mathbf{z}(t)$ and $\mathbf{a}(t)$. Thus, the gradient is computed sequentially without keeping $\mathbf{a}(t)$ and $\mathbf{z}(t)$ for each t , so memory usage can be reduced as well. Based on the above-mentioned properties of ODENet, the benefit against the original ResNet is that the number of parameters can be reduced by ODENet. In the prediction process, ResNet is represented with M different building blocks, while ODENet repeatedly uses a single ODEBlock M times. When the number of parameters for one building block is $O(L)$, those of ResNet and ODENet are $O(LM)$ and $O(L)$, respectively. As we will see in Table 2, the number of parameters for pre- and post-processing layers (e.g., conv1 and fc) is not significant, it is expected that the number of parameters of ResNet is reduced to approximately $\frac{1}{M}$. In other words, different parameters are used for each t in ResNet, as shown in Equation 1. In ODENet, on the other hand, as shown in Equation 2, θ is independent of t ; thus, it can be trained while the parameters are fixed irrespective of t . Please note that different ODE solvers can be used in prediction and training processes. For example, a fourth-order Runge-Kutta method is used for training with high accuracy, while Euler method is used for prediction tasks for low latency and simplicity. We can strike a balance between accuracy and performance by selecting a proper solver.

2.4 ANODE

One of issues of ODENet is that there is a possibility that gradients cannot be computed accurately during the training phase. For sake of simplicity, as shown in Equation 10, we assume one-step Euler method and $z(t)$ is a scalar.

$$z(t_1) = z(t_0) + f(z(t_0), \theta), \quad (10)$$

where $z(t_0), z(t_1) \in \mathbb{R}$.

Gradient of $z(t_0)$ in Equation 10 is computed based on the chain rule as follows.

$$\frac{\partial J}{\partial z(t_0)} = \frac{\partial J}{\partial z(t_1)} \left(1 + \frac{\partial f}{\partial z(t_0)}\right) \quad (11)$$

On other hand, the gradient computed approximately by the adjoint method is as follows.

$$\frac{\partial J}{\partial z(t_0)} = -\frac{\partial J}{\partial z(t_1)} \left(1 + \frac{\partial f}{\partial z(t_1)}\right) \quad (12)$$

The differences between Equations 11 and 12 are accumulating during the training phase, and thus there is a possibility that gradients cannot be computed accurately in ODENet.

ANODE can address this issue by introducing a checkpointing technique. Let M , $z(t_0)$, and $z(t_i)$, $i \in [1, M]$ be the number of building blocks, input of the first building block, and the output of the i -th building block, respectively. Algorithm 1 shows the training process of ANODE.

Algorithm 1 increases the memory size during the training phase from $O(L)$ to $O(L) + O(H)$, where H is the number of repeated steps of Euler method (i.e., reciprocal of the step size h in Equation 5). Please note that prediction process of ANODE is same as that of ODENet. In this paper, ODEBlock trained by Algorithm 1 is denoted as ANODEBlock.

3 FPGA Implementation

3.1 ODEBlock

In this paper, as a target platform, we employ SoC type FPGA devices that integrate programmable logic (PL) part and processor (PS) part, as shown in Figure 3. PS part consists of CPU and DRAM, while PL part has programmable logic.

Algorithm 1 Training process of ANODE

- 1: **Forward**
- 2: Keep the values of $\forall j \in [0, M], z(t_j)$
- 3: **Backward**
- 4: Initialize gradients
- 5: **for** $k \in M \cdots 1$ **do**
- 6: Recompute the local computation graph from $z(t_{k-1})$ to $z(t_k)$ using k -th building block
- 7: Compute gradients according to the local computation graph
- 8: Update the gradients
- 9: Free the local computational graph
- 10: **end for**

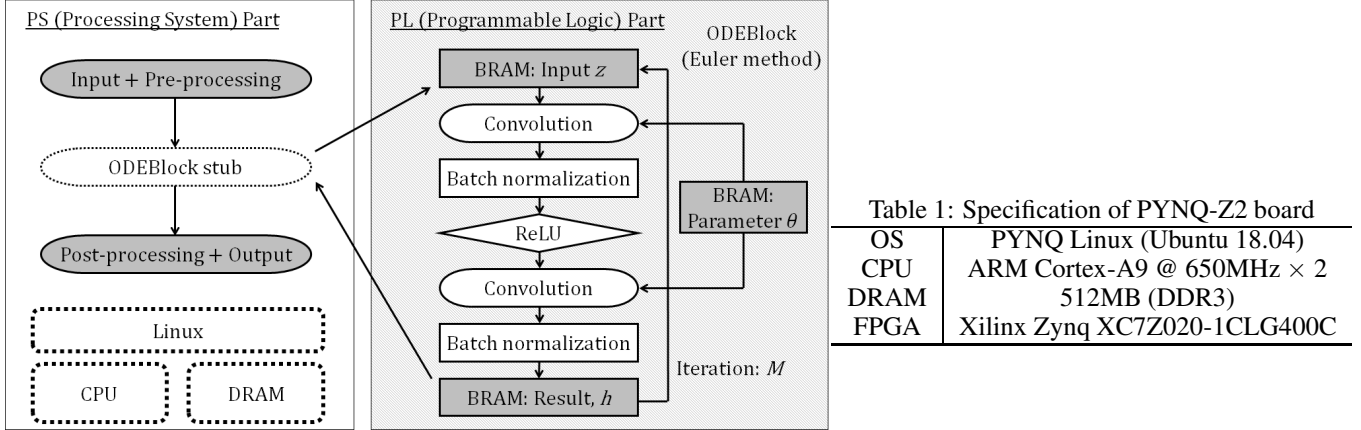


Figure 3: ODEBlock design on FPGA

We use TUL PYNQ-Z2 board [13] in this paper. Table 1 shows the specification. As shown in Figure 3, a part of the ODEBlock is implemented on PL part as a dedicated circuit, while the others are executed on PS part as software.

Table 2 shows network structures of ODENet and ANODE with a given N . It consists of several building blocks or “layers” as shown in the table: conv1, input1, input2_1, input2_2, input3_1, input3_2, and fc. In the case of ODENet, only a single block instance is implemented for each layer, and the same instance is continuously executed instead. For example, the numbers of executions per block for input1, input2_2, and input3_2 are $\frac{N-2}{6}$, $\frac{N-8}{6}$, and $\frac{N-8}{6}$, respectively; the others are executed only once. In this paper, we thus implement input1, input2_2, and input3_2 individually on a resource-limited FPGA board. That is, each of these layers is implemented on PL part of PYNQ-Z2, while the other parts are executed on PS part as software. Euler method is used as an ODE solver.

Each layer consists of five steps: 1) convolution, 2) batch normalization, 3) activation function (ReLU), 4) convolution, and 5) batch normalization. The convolution step differs in each layer. That is, the input/output channel numbers for layer1, layer2_2, and layer3_2 are 16, 32, and 64. The input/output feature map sizes for layer1, layer2_2, and layer3_2 are 8×8 , 16×16 , and 32×32 . Their kernel size is 3×3 and stride width is 1. The above mentioned five steps are implemented in Verilog HDL. 32-bit Q20 fixed-point number format is used. Multiply-add units are used in the convolution and ReLU steps, and multiply-add units, division unit, and square root unit are used in the batch normalization steps for computing mean, variance, and standard deviation. Weight parameters θ of the two convolution steps are stored in Block RAM (BRAM) of the FPGA. Input and output feature maps for all the channels are also stored in the BRAM.

Most of computation time is consumed in the convolution steps². Our convolution and ReLU step implementations are scalable; that is, we can increase the number of multiply-add units from 1 to 64 depending on available resources but it is also restricted by the number of output channels. Their execution cycles (except for the batch normalization) decrease in inverse proportion to the number of multiply-add units. We implemented layer1, layer2_2, and layer3_2 each using 1, 4, 8, 16, and 32 multiply-add units. They are referred to as conv_x1, conv_x4, conv_x8, conv_x16, and conv_x32, respectively. For example, their execution cycles of layer3_2 are 23.78M, 6.07M, 3.12M, 1.64M, and

²The two convolution steps consume about 99% of execution cycles of layer3_2 when only a single multiply-add unit is used in our implementation.

Table 2: Network structure of ODENet and ANODE

Layer	Output size	Detail	Param size [kB]	# of exec per block
conv1	$32 \times 32, 16\text{ch}$	3×3 , stride 1	1.86	1
layer1	$32 \times 32, 16\text{ch}$	$\begin{matrix} 3 \times 3 \\ 3 \times 3 \end{matrix}$, stride 1	19.84	$\frac{N-2}{6}$
layer2_1	$16 \times 16, 32\text{ch}$	$\begin{matrix} 3 \times 3 \\ 3 \times 3 \end{matrix}$, stride 2	55.81	1
layer2_2	$16 \times 16, 32\text{ch}$	$\begin{matrix} 3 \times 3 \\ 3 \times 3 \end{matrix}$, stride 1	76.54	$\frac{N-8}{6}$
layer3_1	$8 \times 8, 64\text{ch}$	$\begin{matrix} 3 \times 3 \\ 3 \times 3 \end{matrix}$, stride 2	222.21	1
layer3_2	$8 \times 8, 64\text{ch}$	$\begin{matrix} 3 \times 3 \\ 3 \times 3 \end{matrix}$, stride 1	300.54	$\frac{N-8}{6}$
fc	1×100	Average pooling, 100d fc, softmax	26.00	1

Table 3: Resource utilizations of layer1, layer2_2, and layer3_2 on Zynq XC7Z020

Layer	Parallelism	BRAM		DSP		LUT		FF	
layer1	conv_1	56	(40.00%)	8	(3.63%)	1486	(2.79%)	835	(0.78%)
	conv_4	56	(40.00%)	20	(9.09%)	2992	(5.62%)	1358	(1.28%)
	conv_8	56	(40.00%)	36	(16.36%)	4740	(8.91%)	2058	(1.93%)
	conv_16	64	(45.71%)	68	(30.91%)	8994	(16.91%)	4145	(3.90%)
layer2_2	conv_1	56	(40.00%)	8	(3.63%)	1482	(2.79%)	833	(0.78%)
	conv_4	56	(40.00%)	20	(9.09%)	2946	(5.53%)	1346	(1.27%)
	conv_8	56	(40.00%)	36	(16.36%)	4737	(8.90%)	2032	(1.91%)
	conv_16	56	(40.00%)	68	(30.91%)	8844	(16.62%)	4873	(4.58%)
layer3_2	conv_1	140	(100.00%)	8	(3.63%)	1692	(3.18%)	927	(0.87%)
	conv_4	140	(100.00%)	20	(9.09%)	3048	(5.73%)	1411	(1.33%)
	conv_8	140	(100.00%)	36	(16.36%)	4907	(9.22%)	2059	(1.94%)
	conv_16	140	(100.00%)	68	(30.91%)	12720	(23.91%)	6378	(5.99%)

0.90M cycles, respectively. In these implementations, since only conv_x32 could not satisfy a timing constraint of our target FPGA board (i.e., 100MHz), we mainly use conv_x16 in this paper.

3.2 Resource Utilization

Table 3 shows resource utilizations of layer1, layer2_2, and layer3_2 implemented on PL part of the FPGA for ODENet, ANODE, and their variants in this paper. Here, we show the result when n multiply-add units are used for the convolution and ReLU steps. They are denoted as conv_xn implementations. As shown in the table, if we implement layer3_2 on PL part of the FPGA, BRAM utilization becomes 100%. In this case, the utilizations of DSP, LUT, and FF still have room and can implement some other application logic, but we cannot implement more weight parameters or larger feature maps without relying on external DRAMs. On the other hand, BRAM utilizations of layer1 and layer2_2 are not as high as layer3_2, and the other resources also have enough room, so we can implement both the layers on PL part of the FPGA. In the next section, we can thus consider four cases: 1) only layer1 is implemented on PL part, 2) only layer2_2 is implemented on PL part, 3) layer1 and layer2_2 are implemented on PL part, and 4) only layer3_2 is implemented on PL part of the FPGA.

4 Evaluations

CIFAR-100 is used as a dataset in this paper. ODENet, ANODE, and their variants on the FPGA is evaluated in terms of the number of parameters, accuracy, and execution time when a part of convolution layers is executed by PL part.

4.1 Network Configuration

Here, we introduce reduced ODENet (rODENet) and reduced ANODE (rANODE) variants for low-cost FPGA implementation. As shown in Table 4, thirteen network architectures including our rODENet and rANODE variants listed below are used in this evaluation. Please note that the number of stacked blocks means the number of block instances implemented, while the number of executions per block means the number of iterations on the same block instance.

- **ResNet-N**: Baseline ResNet
- **ODENet-N**: layer1, layer2_2, and layer3_2 in **ResNet-N** are replaced with corresponding ODEBlocks.
- **ANODE-N**: Same architecture as **ODENet-N** but using ANODEBlocks instead of ODEBlocks
- **rODENet-1-N**: layer2_2 and layer3_2 are removed. layer1 is replaced with ODEBlock, and the number of executions on layer1 is increased instead so that the total execution count of building blocks is same as **ResNet-N**.
- **rANODE-1-N**: Same architecture as **rODENet-1-N** but using ANODEBlocks instead of ODEBlocks
- **rODENet-2-N**: The number of executions on layer1 is reduced to 1 and layer3_2 is removed. layer2_2 is replaced with ODEBlock, and the number of executions on layer2_2 is increased instead.
- **rANODE-2-N**: Same architecture as **rODENet-2-N** but using ANODEBlocks instead of ODEBlocks
- **rODENet-1+2-N**: layer3_2 is removed. layer1 and layer2_2 are replaced with ODEBlocks, and the numbers of executions on layer1 and layer2_2 are increased instead.
- **rANODE-1+2-N**: Same architecture as **rODENet-1+2-N** but using ANODEBlocks instead of ODEBlocks
- **rODENet-3-N**: The number of executions on layer1 is reduced to 1 and layer2_2 is removed. layer3_2 is replaced with ODEBlock, and the number of executions on layer3_2 is increased instead.
- **rANODE-3-N**: Same architecture as **rODENet-3-N** but using ANODEBlocks instead of ODEBlocks
- **hODENet-3-N**: Only layer3_2 in **ResNet-N** is replaced with ODEBlock. The other layers are the same as those in ResNet. It is hybrid between ResNet and ODENet.
- **hANODE-3-N**: Same architecture as **hODENet-3-N** but using ANODEBlocks instead of ODEBlocks

We can expect that computations of **ODENet-N** and its ANODE variant are compatible with that in **ResNet-N**. On the other hand, our **rODENet-1-N**, **rODENet-2-N**, **rODENet-1+2-N**, **rODENet-3-N**, and their ANODE variants execute the same number of building blocks as **ResNet-N**, but they heavily use layer1, layer2_2, layer1 and layer2_2, and layer3_2, respectively.

Our intention is that these heavily-used layers are offloaded to PL part as shown in Figure 3. In addition, **hODENet-3-N**, which is a middle of **ResNet-N** and **ODENet-N**, is evaluated as a high-accuracy variant.

Euler method is used as an ODE solver, because it is simple and requires only a small temporary memory at prediction time. In Table 4, conv1 is the pre-processing step that executes 3×3 convolution, batch normalization, and ReLU as an activation function. Then, various building blocks (e.g., layer1 to layer3_2 in Table 4) are executed as shown in Figure 1. Finally, fc is the post-processing step that executes global average pooling, fully-connected layer to all the output classes, and Softmax as an activation function. Stride width is set to 1 in most of building blocks except for layer2_1 and layer3_1, in which stride width is set to 2 in order to reduce the output feature map size.

4.2 Parameter Size

Figure 4 shows the total parameter size for each architecture listed in Section 4.1, assuming that each parameter is implemented in a 32-bit format. As shown in Figure 4, parameter sizes of ANODE and rANODE variants are same as those of corresponding ODENet and rODENet variants. Thus, we focus on parameter sizes of ODENet variants in the following discussion.

As shown in Table 4, parameter size of **ResNet-N** is proportional to the number of stacked building blocks (see Figure 1). Please note that parameter sizes of ODENet and rODENet variants are independent of N, since the number of stacked instances is independent of N (see Figure 2). In the rODENet variants, their parameter sizes depend on layers actually implemented. When N is 20 (the smallest case), parameter sizes of **ODENet-N** and **rODENet-3-N** are 36.24% and 43.29% less than that of **ResNet-20**, respectively. When N is 56 (the largest case), their parameter sizes are 79.54% and 81.80% less than that of **ResNet-56**, respectively. Although structure of **hODENet-3-N** is similar to that of **ResNet-N** except for layer3_2, it can reduce the parameter size by 26.43% and 60.16% compared to **ResNet-N** when N is 20 and 56, respectively. Please note that the parameter size reduction by using ODEBlock is independent

Table 4: Network structure of ResNet, ODENet, and rODENet variants

Layer	Output size	Detail	# of stacked blocks / # of executions per block						
			ResNet	ODENet ANODE	rODENet-1 rANODE-1	rODENet-2 rANODE-2	rODENet-1+2 rANODE-1+2	rODENet-3 rANODE-3	hODENet-3 hANODE-3
conv1	$32 \times 32, 16\text{ch}$	3×3 , stride 1	1 / 1	1 / 1	1 / 1	1 / 1	1 / 1	1 / 1	1 / 1
layer1	$32 \times 32, 16\text{ch}$	3×3 , stride 1	$\frac{N-2}{6} / 1$	$1 / \frac{N-2}{6}$	$1 / \frac{N-6}{2}$	1 / 1	$1 / \frac{N-4}{4}$	1 / 1	$\frac{N-2}{6} / 1$
layer2_1	$16 \times 16, 32\text{ch}$	3×3 , stride 2	1 / 1	1 / 1	1 / 1	1 / 1	1 / 1	1 / 1	1 / 1
layer2_2	$16 \times 16, 32\text{ch}$	3×3 , stride 1	$\frac{N-8}{6} / 1$	$1 / \frac{N-8}{6}$	0 / 0	$1 / \frac{N-8}{2}$	$1 / \frac{N-8}{4}$	0 / 0	$\frac{N-8}{6} / 1$
layer3_1	$8 \times 8, 64\text{ch}$	3×3 , stride 2	1 / 1	1 / 1	1 / 1	1 / 1	1 / 1	1 / 1	1 / 1
layer3_2	$8 \times 8, 64\text{ch}$	3×3 , stride 1	$\frac{N-8}{6} / 1$	$1 / \frac{N-8}{6}$	0 / 0	0 / 0	0 / 0	$1 / \frac{N-8}{2}$	$1 / \frac{N-8}{6}$
fc	1×100	Average pooling, 100d fc, softmax	1 / 1	1 / 1	1 / 1	1 / 1	1 / 1	1 / 1	1 / 1

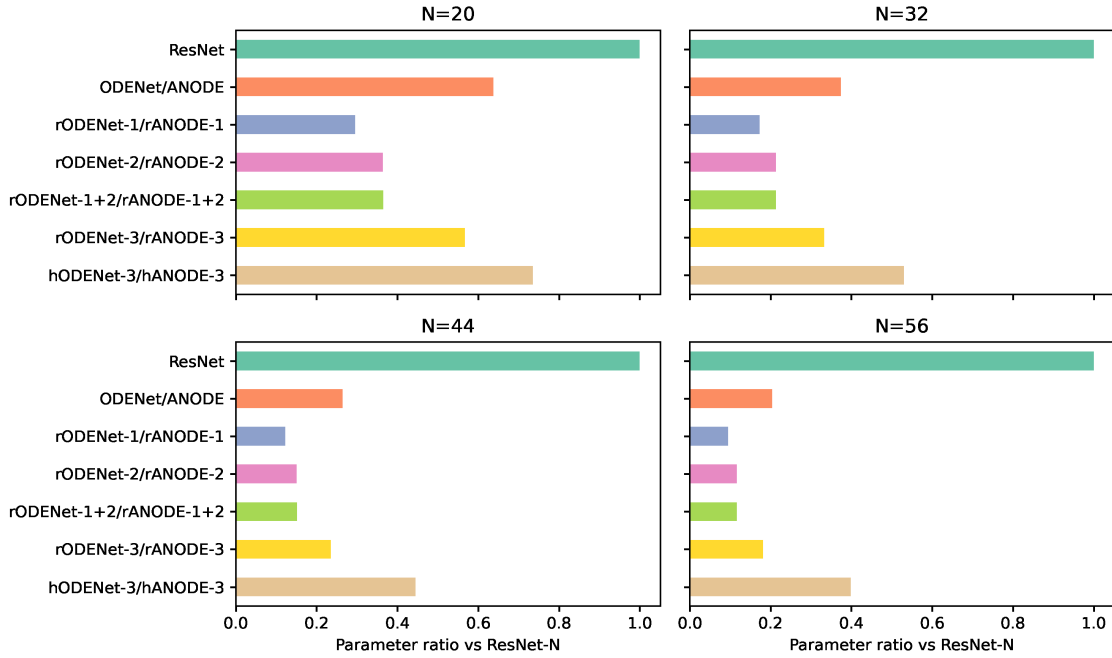


Figure 4: Parameter size of ResNet, ODENet, and rODENet variants

of the other parameter reduction techniques, such as quantization [6], and can be incorporated with them to further reduce the parameter size.

4.3 Accuracy

In this experiment, SGD [14] is used as an optimization function. As L2 regularization, 1×10^{-4} is added to each layer. For the training process, the number of epochs is 200. The learning rate is started with 0.1, and it is reduced by $\frac{1}{10}$ when the epoch becomes 100 and 150.

Figure 5 shows the evaluation results of accuracy in the thirteen network architectures listed in Table 4. In Figure 5, ODENet and rODENet variants are shown in solid lines while their ANODE versions are shown in dotted lines. As shown in the graphs, when N is 20, the training results are unstable especially in **ODENet-N** and **hODENet-3-N**. When N is 56, on the other hand, accuracies of most architectures are improved and become stable, except for **rODENet-1-N** and **rODENet-1+2-N**. ANODEBlock based architectures tend to acquire higher accuracy than ODEBlock based ones.

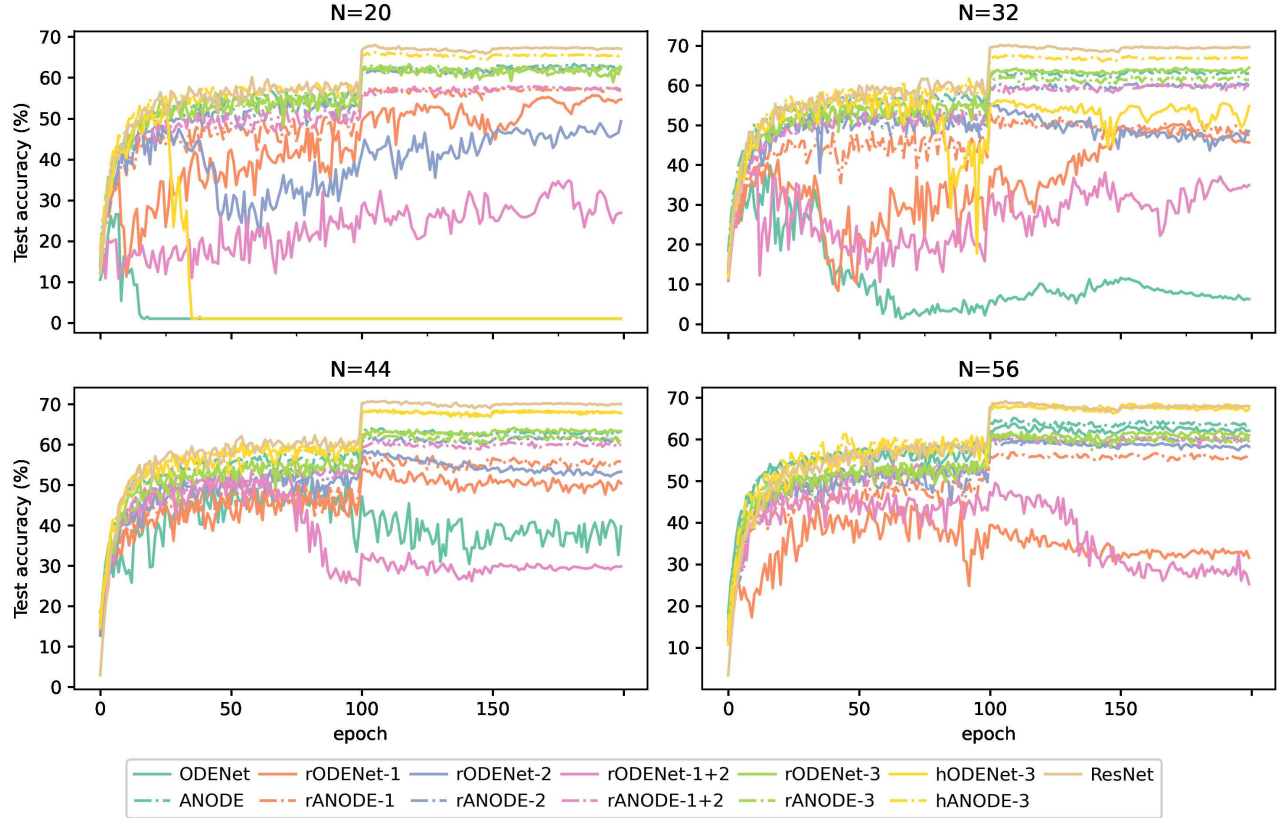


Figure 5: Accuracy of thirteen network architectures when $N=\{20,32,44,56\}$

Among the rODENet variants, **rODENet-3** is stable and shows relatively high accuracy when N is 20, 32, 44, and 56. Likewise, **rANODE-3-N** shows the best accuracy among the other rANODE variants except when N is 56 (it is still the second highest when N is 56). In the following discussion, we thus mainly focus on **rODENet-3** and **rANODE-3**.

In **hODENet-3-N**, the accuracy is the almost same as **ResNet-N** when N is 44 and 56. More specifically, accuracies of **ResNet-44** and **hODENet-3-44** are 70.74% and 68.58%, and those of **ResNet-56** and **hODENet-3-56** are 69.09% and 68.11%; thus there is up to 2.16% accuracy loss.

hANODE-3-N is mostly better than **hODENet-3-N** and more stable as shown in Figure 5. Especially, **hANODE-3-20** acquires 12.48% higher accuracy compared to **hODENet-3-20**.

In **rODENet-3-N**, the accuracy is the next to those of **ResNet-N** and **hANODE-3-N** when N is 32. Accuracies of **ResNet-20** and **rODENet-3-20** are 68.02% and 62.54%, and the accuracy difference is 5.48%. Those of **ResNet-32** and **rODENet-3-32** are 70.16% and 64.46%, and the difference is 5.70%. These differences become large compared to those of **hODENet-3-N** and **hANODE-3-N** when N is 44 and 56. Still, **rODENet-3-N** is stable for all the sizes, which means that this architecture has the highest robustness against increasing N among the rODENet variants. Because of its stability, we can use **rODENet-3-N** even if the optimal network architecture is not known yet.

rANODE-3-N is better than **rODENet-3-N** when N is 20 while it is slightly lower than **rODENet-3-N** for the other sizes (e.g., **rANODE-3-44** and **rANODE-3-56** are 0.86% and 0.85% lower than **rODENet-3-44** and **rODENet-3-56**, respectively). Overall, it is still comparable to **rODENet-3-N**.

In **ODENet-N**, the accuracy is 63.85%, which is relatively high when N is 56. However, it is unstable when N is small. The reason for this instability is that the step size was relatively large and thus it could not acquire the dynamics sufficiently. In ODENet and its variants, it is interpreted that connections of ResNet layers are continuous. It is pointed out that there may be a possibility that ODENet cannot compute the gradients accurately. This may be one reason for the instability when N is small.

Table 5: Execution time of ResNet, ODENet, and rODENet variants (PS: Cortex-A9 @650MHz, PL: @100MHz)

Model		Offloaded target	Total w/o PL [s]	Target w/o PL [s]	Ratio of target	Target w/ PL [s]	Total w/ PL [s]	Overall speedup
ResNet	N=20	-	0.54	-	-	-	-	-
	N=32		0.89	-	-	-	-	-
	N=44		1.24	-	-	-	-	-
	N=56		1.58	-	-	-	-	-
rODENet-1 / rANODE-1	N=20	layer1	0.57	0.44	76.89%	0.15	0.28	1.99
	N=32		0.94	0.81	86.06%	0.29	0.42	2.26
	N=44		1.30	1.17	89.91%	0.42	0.55	2.37
	N=56		1.67	1.54	92.14%	0.55	0.68	2.45
rODENet-2 / rANODE-2	N=20	layer2_2	0.52	0.33	63.82%	0.11	0.30	1.75
	N=32		0.86	0.67	77.74%	0.22	0.41	2.08
	N=44		1.19	1.00	84.14%	0.33	0.52	2.28
	N=56		1.52	1.33	87.46%	0.44	0.63	2.40
rODENet-1+2 / rANODE-1+2	N=20	layer1 / layer2_2	0.55	0.25 / 0.17	44.98% / 31.09%	0.09 / 0.06	0.27	1.99
	N=32		0.89	0.42 / 0.33	47.54% / 37.71%	0.15 / 0.11	0.39	2.24
	N=44		1.23	0.60 / 0.50	48.63% / 40.75%	0.22 / 0.17	0.52	2.38
	N=56		1.60	0.81 / 0.66	50.40% / 41.45%	0.29 / 0.22	0.64	2.52
rODENet-3 / rANODE-3	N=20	layer3_2	0.54	0.35	64.48%	0.10	0.29	1.85
	N=32		0.88	0.69	78.44%	0.20	0.39	2.26
	N=44		1.23	1.04	84.44%	0.30	0.49	2.50
	N=56		1.57	1.38	87.87%	0.40	0.59	2.66
ODENet-3 / ANODE-3	N=20	layer3_2	0.56	0.12	21.24%	0.03	0.47	1.18
	N=32		0.90	0.23	25.83%	0.07	0.74	1.23
	N=44		1.25	0.34	27.67%	0.10	1.00	1.24
	N=56		1.60	0.46	28.98%	0.13	1.27	1.26
hODENet-3 / hANODE-3	N=20	layer3_2	0.53	0.12	22.38%	0.03	0.44	1.19
	N=32		0.88	0.23	26.65%	0.07	0.71	1.24
	N=44		1.23	0.35	28.11%	0.10	0.99	1.25
	N=56		1.56	0.46	29.64%	0.13	1.23	1.27

ANODE-N is an architecture that addresses the above mentioned issue. Actually, its accuracy is higher than that of **ODENet-N**. Especially, accuracy of **ODENet-20** is 26.58% while that of **ANODE-20** is 63.35%, which means a significant improvement when N is small, while the parameter size of ANODE is larger than those of **rODENet** and **rANODE** variants.

In summary, our **rODENet-3** and **rANODE-3** are stable and shows relatively high accuracy for all the sizes in our experiment. Considering the parameter size, they can strike a balance between the parameter size reduction, stability, and accuracy.

4.4 Execution Time

The ODENet variants implemented on the FPGA mentioned in Section 3 are evaluated in terms of prediction time. Please note that parameter sizes of ANODE variants are same as those of corresponding ODENet variants, and their execution times of prediction are theoretically the same. We actually implemented ANODE variants on the FPGA board and confirmed that differences between their prediction times are less than 0.01 seconds. We thus mainly focus on prediction times of ODENet variants instead of ANODE variants. More specifically, the following architectures are compared.

- **ResNet-N**: In ResNet-N, all the layers are executed on PS part as software.
- **rODENet-*-N**: In the rODENet variants, only heavily-used layers are offloaded to PL part as dedicated circuits. The other layers are software. Among rODENet variants, we mainly focus on **rODENet-3-N** since it is advantageous in terms of the accuracy. In this case, layer3_2 is PL part and the others are PS part.
- **ODENet-3-N**: In ODENet-N, layer3_2 is PL part and the others are PS part.
- **hODENet-3-N**: In hODENet-3-N, layer3_2 is PL part and the others are PS part.

An image size in CIFAR-100 dataset is (channel, height, width) = (3, 32, 32), and prediction time for each image is measured. As an FPGA platform, TUL PYNQ-Z2 board that integrates PS and PL parts is used in this experiment. As listed in Table 1, in PS part, two ARM Cortex-A9 processors are running at 650MHz. In PL part, the operating frequency of the dedicated circuits is 100MHz. Vivado 2017.2 was used for the design synthesis and implementation of the ODEBlocks (i.e., layer1, layer2_2, and layer3_2) implemented on PL part. We employ conv_x16 implementation that uses 16 multiply-add units for the convolution and ReLU steps. PS and PL parts are typically connected via AXI bus and DMA transfer is used for their communication though not fully implemented in our design. We assume that data transfer latency between PS and PL parts is 1 cycle per float32. This is an optimistic assumption, but we use this value for simplicity because it varies depending on an underlying hardware platform.

Table 5 shows the execution times and speedup rates of the thirteen architectures mentioned above when they are implemented on the FPGA board. In this table, ‘‘Offloaded target’’ means layer(s) implemented on PL part of the FPGA. For example, the offloaded target is layer3_2 in **rODENet-3-N**, **ODENet-3-N**, and **hODENet-3-N**. As shown in the table, execution time of layer3_2 takes up only 21.24% to 29.64% of total execution time of **ODENet-3-N** and **hODENet-3-N**. On the other hand, layer3_2 is heavily used intentionally in **rODENet-3-N**, and its execution time takes up 64.48% to 87.87%. Thus, by offloading layer3_2 to PL part, the total execution time of **rODENet-3-N** is 2.66 times faster than a pure software execution when N is 56, which is the largest overall speedup by the FPGA.

Regarding **hODENet-3-N** and **ODENet-3-N**, the overall speedup by the FPGA for **hODENet-3-N** is marginally higher than that of **ODENet-3-N** in all the sizes. This is because the ratio of layer3_2 in **hODENet-3-N** is slightly higher than that in **ODENet-3-N** and the speedup rate of only layer3_2 by the FPGA is almost constant regardless of N.

In summary, the overall speedup rate by the FPGA is relatively high in the rODENet variants, followed by **hODENet-3-N** and **ODENet-3-N**. Although all the rODENet variants show favorable speedup, **rODENet-3-N** shows high and stable accuracy, as shown in Section 4.3. Regarding the overall speedup compared to the original ResNet, **rODENet-3-56** is 2.67 times faster than a pure software execution of **ResNet-56**. Although the overall speedup by the FPGA is smallest in **ODENet-3-20**, it is still 1.15 times faster than a software execution of **ResNet-20**.

As shown in Section 4.3, accuracy of **rODENet-3-N** is higher than those of rODENet variants, and **rANODE-3-N** is better than **rODENet-3-N** when N is 20. As mentioned, parameter size and prediction time of **rODENet-3-N** and **rANODE-3-N** are the same, we can select **rODENet-3-N** or **rANODE-3-N** depending on the network size. Thus, our proposed **rODENet-3-N** and **rANODE-3-N** would be practical choices in terms of the parameter size, accuracy, stability, and execution time.

5 Summary

To offload a part of ResNet building blocks on PL part of low-cost FPGA devices, in this paper we focused on ODENet and ANODE and they were redesigned. More specifically, as ODENet variants, reduced ODENets (rODENets) each of which heavily uses a part of ODEBlocks and reduces/eliminates some layers differently were proposed and analyzed for low-cost FPGA devices. In addition, rANODE variants, in which ODEBlocks are replaced with ANODEBlocks, were designed to improve stability of the training phase of ODENet. We examined thirteen network architectures including the original ResNet (**ResNet-N**), the original ODENet (**ODENet-N**), the original ANODE (**ANODE-N**), and our proposed rODENet/rANODE variants (e.g., **rODENet-3/rANODE-3-N**) in terms of the parameter size, accuracy, and execution time. A part of ODEBlocks and ANODEBlocks, such as layer1, layer2_2, and layer3_2, was implemented on PL part of PYNQ-Z2 board to evaluate their FPGA resource utilization. For example, **rODENet-3-N** and **rANODE-3-N** heavily use layer3_2, reduces layer1, eliminates layer2_2, and offloads layer3_2 to PL part of the FPGA. The evaluation results using CIFAR-100 dataset showed that the parameter sizes of **rODENet-3 (rANODE-3)-N** are 43.29%, and 81.80% less than those of **ResNet-N** when N is 20 and 56, respectively. Although accuracies of rODENet and rANODE variants are not higher than ResNet, hODENet, and hANODE, accuracies of **rODENet-3-N** and **rANODE-3-N** are stably high compared to the others in most cases. **rANODE-3-N** is better than **rODENet-3-N** when N is 20, so we can select one of them depending on the network size. **rODENet-3-N (rANODE-3-N)** is 2.66 times faster than a pure software execution when N is 56, which is the largest overall speedup by the FPGA. It is 2.67 times faster than a software execution of **ResNet-N** when N is 56. In summary, our proposed **rODENet-3-N** and **rANODE-3-N** can strike a balance between the parameter size, accuracy, stability, and execution time.

As a future work, although we used 32-bit fixed-point numbers in this paper, we are planning to use reduced bit widths (e.g., 16-bit or less) in order to implement more layers in PL part to further improve the performance.

References

- [1] Kaiming He, Xiangyu Zhang, Shaoqing Ren, and Jian Sun. Deep Residual Learning for Image Recognition. In *Proceedings of the IEEE Conference on Computer Vision and Pattern Recognition (CVPR'16)*, pages 770–778, Jun 2016.
- [2] Ricky T. Q. Chen, Yulia Rubanova, Jesse Bettencourt, and David Duvenaud. Neural Ordinary Differential Equations. In *Proceedings of the Annual Conference on Neural Information Processing Systems (NeuroIPS'18)*, pages 6572–6583, Dec 2018.
- [3] Amir Gholaminejad, Kurt Keutzer, and George Biros. ANODE: Unconditionally Accurate Memory-Efficient Gradients for Neural ODEs. In *Proceedings of the International Joint Conference on Artificial Intelligence (IJCAI'19)*, pages 730–736, Aug 2019.
- [4] Sergey Ioffe and Christian Szegedy. Batch Normalization: Accelerating Deep Network Training by Reducing Internal Covariate Shift. In *Proceedings of the International Conference on Machine Learning (ICML'15)*, pages 448–456, Jul 2015.
- [5] Hirohisa Watanabe and Hiroki Matsutani. Accelerating ODE-Based Neural Networks on Low-Cost FPGAs. In *Proceedings of the International Parallel and Distributed Processing Symposium Workshops (IPDPSW'21)*, pages 88–95, May 2021.
- [6] Kaiyuan Guo, Shulin Zeng, Jincheng Yu, Yu Wang, and Huazhong Yang. A Survey of FPGA-Based Neural Network Accelerator. *arXiv:1712.08934v3*, Dec 2018.
- [7] Julian Faraone, Martin Kumm, Martin Hardieck, Peter Zipf, Xueyuan Liu, David Boland, and Philip H.W. Leong. AddNet: Deep Neural Networks Using FPGA-Optimized Multipliers. *IEEE Transactions on Very Large Scale Integration (VLSI) Systems*, 28(1):115–128, Jan 2020.
- [8] Yufei Ma, Minkyu Kim, Yu Cao, Sarma Vrudhula, and Jae sun Seo. End-to-End Scalable FPGA Accelerator for Deep Residual Networks. In *Proceedings of the International Symposium on Circuits and Systems (ISCAS'17)*, pages 1–4, May 2017.
- [9] Javier Duarte et al. FPGA-Accelerated Machine Learning Inference as a Service for Particle Physics Computing. *Computing and Software for Big Science*, 3(13), Oct 2019.
- [10] Vinod Nair and Geoffrey E Hinton. Rectified Linear Units Improve Restricted Boltzmann Machines. In *Proceedings of the International Conference on Machine Learning (ICML'10)*, pages 807–814, Jun 2010.
- [11] William H. Press, Saul A. Teukolsky, William T. Vetterling, and Brian P. Flannery. *Numerical Recipes. The Art of Scientific Computing, 3rd Edition*. Cambridge University Press, 2007.
- [12] L. S. Pontryagin, V. G. Boltyanskii, R. V. Gamkrelidze, and E. F. Mishechenko. *The Mathematical Theory of Optimal Processes*. John Wiley & Sons, 1962.
- [13] PYNQ - Python Productivity for Zynq. <http://www.pynq.io/>.
- [14] Ohad Shamir and Tong Zhang. Stochastic gradient descent for non-smooth optimization: Convergence results and optimal averaging schemes. In *Proceedings of the International Conference on Machine Learning (ICML'13)*, pages 71–79, Jun 2013.